SPECTROSCOPIC PROPERTIES OF HERBIG-HARO FLOWS

KARL-HEINZ BÖHM
Department of Astronomy, University of Washington
Seattle, Washington 98195, USA

AND

ANTHONY P. GOODSON
Department of Physics, University of Washington
Seattle, Washington 98195, USA

Abstract. While recent studies of Herbig-Haro (HH) objects have focused less on the details of their spectra than on the hydrodynamics of jets and their working surfaces, many open questions concerning these spectra remain. Attempts to quantitatively explain a wide range of lines for many HH objects point to discrepancies between theory and observation. Some lines (specifically [S II](6716+6731)) are much stronger than predicted by simple plane-shock and bow-shock models, while in general high ionization lines (e.g. lines of [O III], [Ne III] and [S III] in the optical and the [C IV] and [N V] in the ultra-violet) are much weaker than expected, pointing to difficulties with current models. On the other hand, examination of these lines has lent new insight into both the quality of our predictions and the nature of HH outflows. Examination of many Fe lines have demonstrated that our ability to estimate abundances from faint lines is surprisingly good (or surprisingly consistent). Position velocity diagrams have also been constructed (using forbidden emission lines), allowing outflows to be mapped to within 0."3 arcseconds of the source star.

1. Introduction

The description and interpretation of spectra originally played a decisive role in the early analysis of Herbig-Haro (HH) objects (Herbig 1951; see also Böhm 1956; Osterbrock 1958 for early attempts to give a quantitative explanation.) Later, the recognition that most HH spectra are generated

B. Reipurth and C. Bertout (eds.), Herbig–Haro Flows and the Birth of Low Mass Stars, 47–62.

by shocks (Schwartz 1975) offered an opportunity to explain their spectra using shock wave models (see e.g. Dopita 1978, Raymond 1979.) The further discovery that the optical spectra of many HH objects are generated in bow-shock like structures (Hartmann & Raymond 1984) encouraged the use of bow shock models to obtain a more detailed understanding of the spectra (see e.g. Hartmann & Raymond 1984; Raga & Böhm 1985, 1986, 1987; Hartigan, Raymond & Hartmann 1987; Raymond, Hartigan & Hartmann 1988.) More recent studies have focused less on the detailed explanation of the spectrum than on the hydrodynamics of the jets and their working surfaces and, if possible, on a hydrodynamical explanation of the images in specific strong lines. There have been relatively few attempts to explain quantitatively a wide range of lines. This is especially true of the many new line identifications which have been made in the last decade. (See e.g. Solf, Böhm & Raga 1988 who found 189 lines for the 3720 Å $< \lambda <$ 10830 Å in HH1.)

This paper addresses our current ability to quantitatively interpret HH spectra, and highlights some of the open questions regarding this interpretation which are applicable to HH objects in general. All discrepancies which are restricted to one or a very few objects are assumed to be related to the specific properties of those particular objects and are of less interest. Our question is: *Do we really understand HH spectra?*

Our main interest is the optical spectra (we define their range as 3700-10830 Å). Because of the close connections with optical spectra we shall also briefly discuss the UV spectra (for HH objects usually measured with IUE) and the near IR H_2 rotation-vibration spectra.

We want to study and (if possible) interpret:

1) The spectrophotometric flux of the lines.

2) The line profiles or the position-velocity diagrams (derived from long-slit spectra).

3) The full appearance (in 2 spatial dimensions) of line profiles as seen e.g. with a Fabry-Perot interferometer.

From our point of view the observations described in 1) are the most important ones. (For example, if the spectrophotometry of a given line disagrees with the models for all HH objects, there is likely something wrong with the basic interpretation.) Observations described in 2) and especially in 3) are more strongly dependent on the geometry of the shock and often require a specific interpretation of the individual object.

The following theoretical models can be and have been used for the interpretation of HH spectra:

1) Plane shocks (useful, easily understood, although in most cases not very realistic.) May be acceptable in some cases with high spatial resolution.

2) "1.5-Dimensional Bow Shock" (a bow shock composed of the superposition of oblique plane shocks.) (Hartmann & Raymond 1984; Raga & Böhm 1985, 1986; Hartigan, Raymond & Hartmann 1987.)

3) 2-Dimensional Bow Shocks (see e.g. Raga & Böhm 1987, Raga *et al.* 1988), asymmetric bow shocks (Henney 1996.)

4) Models (simulations) of working surfaces of jets (including bow shocks and jet shocks) (e.g. Blondin, Königl & Fryxell 1989; Stone & Norman 1993; de Gouveia dal Pino & Benz 1993; Raga 1995.)

5) Internal working surfaces of the jet due to the variability of the sources (Biro & Raga 1994)

6) Other important mechanisms: a) Turbulent mixing (entrainment) layers (Cantó & Raga 1991), especially important for H_2 emission. b) Emission of C-bow shocks or mixed J-C shocks (e.g. Fernandes, Brand & Burton 1995; Davis, Eislöffel & Smith 1996)

2. Some Unsolved Problems of Herbig-Haro Spectra

Any appraisal of the quality of our understanding of HH spectra requires a model which has a wide application, at least in a qualitative context. As stated above, we search not for discrepancies between observation and theory in individual objects (which may be due to using an inappropriate detailed model) but rather for discrepancies for certain lines which apply to all observed objects.

The models described in 1) and 2), which are stationary and require only the knowledge of shock velocity and pre-shock density, are used for the comparison. They permit the prediction of the whole line spectrum without difficulty. Other models are hydrodynamically much more sophisticated (especially 4) and 5)) but have difficulty predicting the full spectrum. A considerable fraction of the comparison with models 1) has been carried out by Raga, Böhm & Cantó (1996).

In the following we discuss unexpected results for the spectrophotometric flux of the lines in the optical spectrum. In our discussion we follow the distinction between high excitation objects (HEO) and low excitation objects (LEO) (Böhm, Brugel & Mannery 1980.) We show in tables 1 and 2 information about the spectrum of HH1 (high excitation object, Solf *et al.* 1988) and HH7 (low excitation object, Böhm & Solf 1990.) We list all detected ions and atoms and indicate the flux of the strongest line of the ion or atom in question. (The fluxes F are listed on the standard relative scale where $F(H_\beta) = 100$.)

The tables show the well-known facts about HH-spectra. In order to show the difference between high and low excitation objects more clearly we have also listed in table 2 (with a minus sign) ions which were not

TABLE 1. HH1: a High Excitation Object

	Optical Lines		UV Lines
Ion(atom)	F($F_{H_\beta} = 100$)	Ion	F($F_{H_\beta} = 100$)
H	311		
HeI	131	*CII*	186
HeII	2	*CIII*	330
[*CI*]	7	*CIV*	416
[*NI*]	16	*NIII*	125
[*NII*]	151	*OIII*	150
[*OI*]	159	*MgII*	163
[*OII*]	135	*SiII*	71
[*OIII*]	57	*SiIII*	70
[*NeIII*]	15	*SiIV*	200
NaI	0.4		
MgI, [*MgI*]	7, 1.2		
[*SII*]	105		
[*SIII*]	6		
[*ClII*]	1.5		
[*ArIII*]	2.4		
[*ArIV*]	0.5		
CaII, [*CaII*]	33, 45		
[*CrII*]	2.3		
[*FeII*]	31		
[*FeIII*]	4		
[*NiII*]	16		

detected in HH7 but are seen in HH1. We indicate some ions or atoms which are not so well-known, like Ar IV, Cl II, and Na I. The presence of Na I in the HH spectrum is surprising and begs the questions: In which region of the shock wave is it formed and is it excited by electron collisions (in spite of the very low ionization energy of Na I)?

An interesting problem is the unusual flux of [C I] 9849 Å in HH7 which is about 150 times as strong as the same line in HH1, a result which is not easily explained in terms of a shock wave model. However, the total line fluxes in low excitation objects are (surprisingly) well explained with low velocity J shocks.

Is the simple separation of HH objects in high and low excitation sufficient? The introduction of a new category, "intermediate excitation objects," is under consideration. Raga *et al.* (1996) suggested this because they found a reasonably large number of HH objects (13 out of 45) which

TABLE 2. HH7: a Low Excitation Object

	Optical Lines		Fluorescent H_2 Lines (not in HH7, but in HH43, HH47)
Ion(atom)	F($F_{H_\beta} = 100$)	Ion	F($F_{H_\beta} = 100$)
H	435		H_2
HeI	–		λ
$HeII$	–		1271
$[CI]$	1059		1431
$[NI]$	286		1461
$[NII]$	34		1489
$[OI]$	577		1505
$[OII]$	–		1547
$[OIII]$	–		1562
$[NeIII]$	–		
NaI	–		
MgI	–		
$[SII]$	754		
$[SIII]$	–		
$[ClII]$	–		
$[ArIII]$	–		
$[ArIV]$	–		
$CaII, [CaII]$	<14, 86		
$[CrII]$	<3		
$[FeII]$	52		
$[FeIII]$	–		
$[NiII]$	27		

seemed to show "high excitation" in the H_α/[S II] (6716+6731) ratio and low excitation in the [O III](5007)/H_β ratio.

There are several features of the spectrophotometry which are not understood for a broad range of HH objects. The first result of this type concerns the overly strong ratio of [S II](6716+6731)/H_α which cannot be understood for the majority of high and intermediate excitation objects in terms of either a plane shock or a 1.5-D bow shock model (Raga *et al.* 1996.) The authors studied 45 HH condensations. In figure 1 we compare the shock velocity determined from different line ratios for plane shock waves for the observed high excitation objects. For most line ratios the resulting shock velocities cluster at $\sim$ 100 km/sec or somewhat below. However, the ratio of [S II](6716+6731)/H_α indicates a shock velocity of between 180 and 400

https://doi.org/10.1017/S0074180900061532 Published online by Cambridge University Press

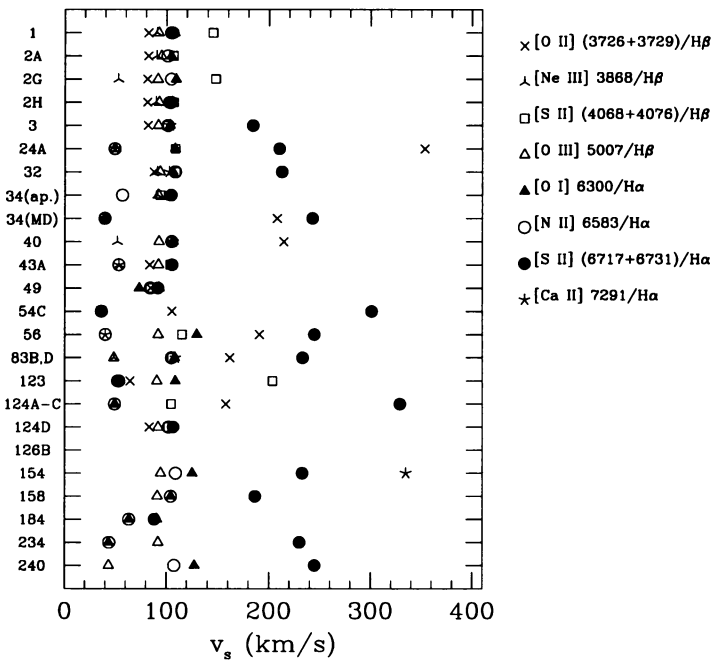

Figure 1. Shock velocities V_s of HEOs as determined from individual line ratios using a plane shock model. Practically all line ratios (and especially [O III]5007/H_β) indicate for all objects $V_s \leq 100$ km/sec. The only major exception is [S II](6717+6731)/H_α which shows for most HEOs a much higher shock velocity. This interpretation persists if bow shock models are used (see fig. 2.) (The high V_s estimate of [O II](3726+3729)/H_β is attributed to contamination of [O II] from background H II regions.) From Raga, Böhm & Cantò (1996.) Courtesy Rev Mex AA.

km/sec. This discrepancy is independent of the type of shock model (plane shock or bow shock) model used, as demonstrated by figure 2.

Most of the observed HEOs show a much larger [S II](6716+6731)/H_α ratio than predicted for these models for the range of shock velocities V_s 50–200 km/sec, which more than spans the range of shock velocities indicated by the other lines (V_s 50−150 km/sec.) The prediction for LEO (e.g. HH11, HH10, HH7, HH34 (jet)) does not lead to comparable contradictions. They are compatible with bow shocks in the range 20-35 km/sec. It is interesting that the discrepancy occurs in the flux ratio [S II](6716+6731)/H_α, which is considered as fundamental for the identification of HH objects.The theory confirms qualitatively the strength of the [S II](6716+6731) in shocks but

https://doi.org/10.1017/S0074180900061532 Published online by Cambridge University Press

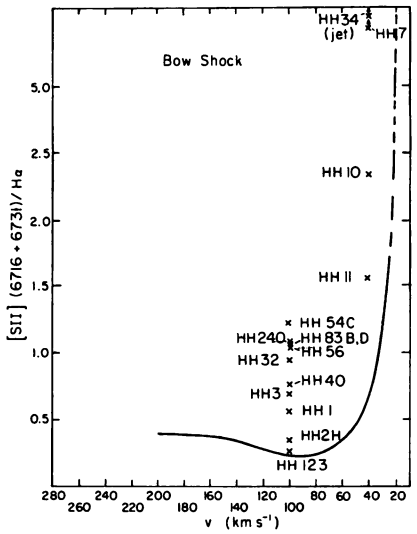

Figure 2. Prediction of the line ratio [SII](6716+6731)/H_α for 1.5-D bow shocks in the range 30 km/sec $\leq V_s \leq$ 200 km/sec (extrapolated to 20 km/sec.) Interpretation of more well-behaved line ratios (not shown) and estimates of total flux require the observational results for the HEOs from HH123 to HH54C to be fitted on the theoretical curve for velocities $\geq$ 100 km/sec. This is obviously impossible. On the other hand the observed LEOs (HH11, HH10, HH7 and HH34 jet) can be fitted easily on the steeply rising part of the theoretical curve in the range 20 km/sec $\leq V_s \leq$ 40 km/sec.

quantitatively the [S II] are considerably stronger than the simple theory predicts. It can be shown, however, that other important low ionization lines (e.g. [O I], measured by the [O I](6300+6363)/H_α ratio) agree very well with the theoretical predictions even in HEOs (Raga *et al.* 1996.)

The next observational result which seems to contradict theoretical expectations is the line ratio [O III](5007)/H_β for HEO. A preliminary discussion of this result was given by Böhm (1995) and Raga *et al.* (1996). Raga *et al.* (1996) plotted the ratio [O III](5007)/H_β as a function of [N I](5200)/H_β. (The latter ratio measures the excitation of the HH object.) In figure 3 we have compared the plot for the observed objects to the theoretical prediction for plane shock waves. The agreement appears reasonable at first sight. However, there is a surprising feature in this diagram. Even the HEOs have an [O III](5007)/H_β ratio which clusters between 0.0 and 0.7, with a definite upper limit among the objects studied so far of [O III](5007)/H_β=1.09. Table 3 shows how surprising this result is from a theoretical viewpoint. The plane and the bow shock models do not at all predict a limit at 1.09. An increase beyond a shock velocity of $\sim$ 120 km/sec would lead to a drastic increase of this ratio, which is seen in no

https://doi.org/10.1017/S0074180900061532 Published online by Cambridge University Press

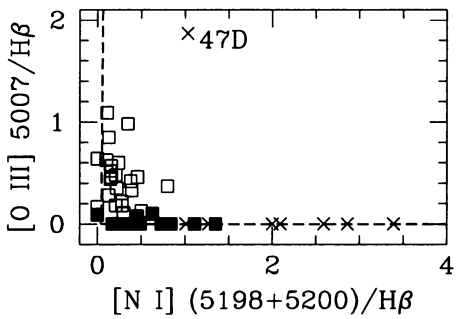

Figure 3. The observed ratio [O III]5007/H_β as a function of excitation, as measured by [N I](5198+5200)/H_β (open squares: HEOs, filled squares: intermediate excitation objects, crosses: LEOs, model prediction: dotted curve.) The line ratio [O III]5007/H_β for the HEOs cluster in the range 0-0.7 and do not become larger than 1.09, in total contradiction with theory (see table 3.) A high value occurs strangely for the LEO(!) HH47D. We follow Dopita *et al.* (1982) and consider this [O III] line strongly influenced by the surrounding H II region. From Raga, Böhm & Cantó (1996). Courtesy Rev Mex AA.

object. Observations show that this effect not only influences [O III]/H_β but also the ratios [Ne III]/H_β and [S III]/H_α. In other words, this effect does not seem to have anything to do with the special properties of the O^{++} ion but rather seems to be a (not yet understood) limitation of high ionization lines in HH objects in general. The result can also be seen in figure 1, where the shock velocities determined from the [O III](5007)/H_β ratio stay at 100 km/sec or below for all HEO.

TABLE 3. Flux ratio $R = [OIII]5007/H_\beta$ for plane and bow shock models

Plane Models		Bow Shock Models	
V_s (km/sec)	R	V_s (km/sec)	R
90	0.07	100	0.43
110	4.17*	150	1.78
		200	2.06

An interesting result which is also visible in the compilation by Raga *et al.* (1996) may throw some additional light on the empirical distinction between HEO and LEO. Raga *et al.* (1996) plotted the average electron density (determined from the ratio (6731)/(6716) of [S II]) as a function of the [N I]5200/H_β ratio and compared this diagram to theoretical plane shock predictions. The theoretical average electron density has been cal-

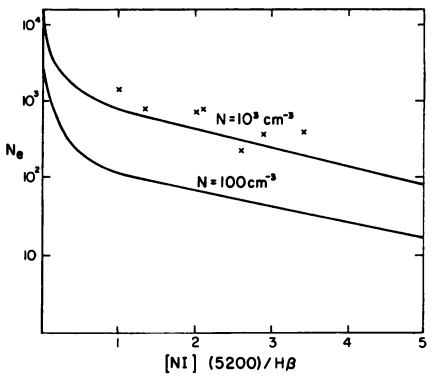

Figure 4. The observed relation between N_e (based on the flux ratio [S II]6731/[S II]6716) and [N I](5198+5200)/H_β for the LEO only, compared to model predictions for a pre-shock density of $N = 100cm^{-3}$ and $N = 1000cm^{-3}$. The extension of the theoretical curves to very high shock velocities (see Raga *et al.* 1996) is not shown (not relevant in the present context.) The figure shows that LEOs have an approximate pre-shock density of $10^3 cm^{-3}$, whereas Raga *et al.* (1996) showed that the HEO and intermediate excitation objects have approximately a pre-shock $N \sim 10^2 cm^{-3}$ (their figure 4b.)

culated from the model results of the (6731)/(6716) ratio and does not use any theoretical input parameters directly. Their result (their figure 4b) shows that the observational results for HEO and most of the intermediate excitation objects are centered around a theoretical curve which is based on a pre-shock density of N=10^2 cm^{-3}. It is interesting that all LEO lie considerably above this curve. In figure 4 we show that all LEO cluster around the curve for a pre-shock N=10^3 cm^{-3}. To first order, this can be treated as an observational selection effect. For a given pre-shock density the (post-shock) N_e declines very rapidly with declining shock velocity. That is especially true for the shock velocity range around 40 km/sec. For the LEO objects we expect (from theoretical models) an N_e of 10-100 cm^{-3} for a pre-shock density of N=10^2 cm^{-3}, meaning that these objects will have a very low surface brightness and are difficult to observe (in comparison to the high excitation objects.) It is therefore not surprising that we discover LEO which have on the average a higher pre-shock density than the HEO. However, there remain two open questions: Why do we not discover HEO which have also a higher pre-shock density ($\sim 10^3$ cm^{-3}), and why do the LEO seem to show an approximately constant pre-shock density of 10^3 cm^{-3}? The answer to these two questions may just be insufficient statistics, although the present results look surprising.

https://doi.org/10.1017/S0074180900061532 Published online by Cambridge University Press

3. The reliability of quantitative spectrophotometry in HH objects and the gas-phase abundances of metals

The study of gas-phase abundances of Fe and Ti in HH-objects (Beck-Winchatz, Böhm & Noriega-Crespo 1996, see below) permits us to make a judgement about the presently achieved accuracy of spectrophotometric data on relatively faint lines in HH objects and the accuracy of abundances derived therefrom. The motivation for this work was as follows: The pre-shock gas-phase metal abundances are likely reduced by binding of the metals in dust grains. The passage of these grains through the HH shock, however, could destroy the dust grains (mostly through sputtering, see e.g. Seab 1987; Draine 1995.) It is to be expected that HEOs, with their high shock velocities, would destroy the dust grains more efficiently than LEOs. This scenario can be checked by determining and comparing the gas-phase metal abundances in LEOs and HEOs. This program has been carried out by Beck-Winchatz *et al.* (1996) (whose results will be quoted below) for a few HH objects.

Our main emphasis here will be on the fact that such observations show us to which degree the spectrophotometry of different moderate faint lines are consistent with each other and what they tell us about the reliability of HH object spectrophotometry and its interpretation. Carrying out this program relies on the comprehensive calculations of the collision strength, especially for Fe^{+}, by Zhang & Pradhan (1995) (see also Bautista & Pradhan 1995.) Fe^{++} are also included, but they are less important and we rely on older data (see Garstang, Robb & Roundtree 1978.) The internal consistency of spectrophotometric data and interpretation are checked in the following way: If the spectrophotometry of the lines is correct, if there are no errors in the collision strengths and transition probabilities, and if the statistical equilibrium and the model of the HH object are strictly correct then we should get exactly the same abundance from any Fe line in a given HH object.

A comparison of the determined Fe abundance from different lines provides an estimate of the magnitude of spectrophotometric and "theoretical" (interpretive) errors, and demonstrates the presently achieved consistency of the spectrophotometric and derived data. In table 4 we show all line fluxes of [Fe II] in HH1 which are larger than 0.02 of the H_β flux and we list the resulting abundance ratio $N(Fe^{+})/N(S^{+})$. We list the lines which deviate in their abundance ratio from the average by less than 20 % with an asterisk (*) and the ones which show a deviation of 20-30% with a cross. There are relatively few lines (4) which show larger deviations and among these are 3 which are relatively high, which might mean that an unrecognized blend is present.

The results of the gas-phase abundance determination of Fe for the

TABLE 4. $N(Fe^+)/N(S^+)$ for HH1 as derived from various lines (natural value *not* logarithm)

Line	F	$N(Fe^+)/N(S^+)$
4276.8	3.6	2.8*
4352.8	2.1	3.43*
4458.0	2.6	2.52+
4814.6	5.5	2.06
4889.6	4.1	2.41+
4905.4	2.0	2.81*
5111.6	3.3	3.8*
5158.8	22.1	2.91*
5261.6	8.9	3.40*
5333.7	4.7	5.13
7637.5	6.8	5.21
8617.0	30.4	3.36*
8891.9	10.0	3.48*
9033.5	2.7	4.40+
9051.9	6.5	3.16*
9267.5	3.9	5.04
	average	3.47
	solar value	2.95

HEOs HH1, HH43A, HH255 and the LEO HH7 and HH11 show unexpected results. (See table 5.) First there are no objects (among these) which show a strongly depleted gas-phase Fe abundance. So, a considerable part of Fe bound up in dust grains must have gone back to the gas phase in all of them. Moreover in our (very restricted) sample there is no fundamental difference between the HEOs and LEOs.

4. Attempts to explain UV and the 2μm IR spectra of H_2

In HEOs more energy is often emitted in the UV spectrum (1200 Å $< \lambda <$ 3000 Å) than in the optical (3700 Å $< \lambda <$ 10830 Å) (Böhm, Böhm-Vitense & Brugel 1980.) Although at first the ionization in the UV seemed to be higher than that in the optical part (Böhm 1983) this does not agree with our present conclusions (see the predictions by Hartigan *et al.* 1987.) We see a similar unexpected behavior of the high ionization lines as was found in the optical. Just as in HEO the [O III] never shows a shock velocity essentially more than $\sim$ 100 km/sec, the same statement applies to the

https://doi.org/10.1017/S0074180900061532 Published online by Cambridge University Press

TABLE 5. $Fe^+/S^+ \sim Fe/S$ in HH Shocks (direct abundance ratio, *not* logarithm)

Sun	2.95
HH1	3.47
HH7*	2.74
HH11*	3.99
HH43A	1.41
HH255 (Burnham's Nebula)	1.05

[C IV] line in the UV. Related to this is the problem that the [N V] line at 1240 Å has never been seen in HH objects (although the prediction for a 160 km/sec shock says that its flux should be 718, compared to 100 for H_β.) It is of great importance but not easy (because of the reddening of HH objects) to obtain improved and reasonably high resolution UV spectra of Herbig-Haro objects.

The UV spectrophotometry of LEO is limited to HH7, HH11, HH43 and HH47 (Cameron & Liseau 1990; Schwartz 1983; Böhm, Scott & Solf 1991.) So far the fluorescent H_2 (pumped by Lyman α) lines (listed in table 2) have been detected in HH43 and HH47. Considerable progress in the interpretation of these interesting lines has been made by Wolfire & Königl (1991.)

The rotation-vibration lines of H_2 in the 2μm region (at least in some cases) are reasonably well predicted by the same models which predict the optical lines. In this context specifically HH32 (Davis, Eislöffel & Smith 1996) and HH1 agree with expectations (Davis, Eislöffel & Ray 1994), because they show that a considerable portion of the H_2 line emission originates in the "wings" of the bow shock. The lack of H_2 emission in the western "wing" of HH1 is understood by the asymmetry of the HH1 bow shock (Solf *et al.* 1991 and especially Henney 1996.) In other cases (e.g. in HH110) a mixing layer (entrainment) can best explain the H_2 emission. (Raga 1995; Noriega-Crespa *et al.* 1996)

5. The explanation of Line Profiles and Position-Velocity Diagrams of HH objects

Considerable progress was achieved in the study of line profiles by Hartigan *et al.* (1987) who pointed out that the bow shock velocity is equal to the measured FWZI (full width at zero intensity) and discussed a number of

objects from this point of view. A study of direct and dust-scattered emission line profiles in the HH1/HH2 system was carried out by Solf & Böhm (1991) who showed that very useful information about the state of motion of these HH objects can be derived from the dust-scattered line profiles originating in front of or behind the HH object. (A preliminary explanation of this result is given by Noriega-Crespo, Calvet & Böhm 1991 and a very detailed and useful theory by Henney *et al.* 1994.)

We have made a considerable effort to explain the observed "position-velocity diagrams" (the spatially dependent line profiles which are obtained from a long slit spectrum, usually but not necessarily along the axis of the HH object, see Raga & Böhm 1985, 1996 and Indebetouw & Noriega-Crespo 1995.) Since the explanations are based on an approximate and geometrically simple bow shock model the agreement is usually acceptable but not ideal. But there are some cases (e.g. HH32, see Solf, Böhm & Raga 1986) where the agreement is impressive. Recently there has been an attempt also to explain the ultraviolet (I.U.E.) "long slit" spectra in a similar way (Moro-Martin *et al.* 1996.)

Following a suggestion of Solf (1989) it has recently become possible to generate position-velocity diagrams of HH jet outflows in the immediate neighborhood of the source stars. (Solf 1989, 1993; Solf & Böhm 1993; Hirth, Mundt & Solf 1994; Hirth 1994; Böhm & Solf 1994; Staude & Elsässer 1993.) The method is based on using long slit spectra taken under different position angles centered on the source star (usually a *T Tauri* star.) The photospheric contribution to the spectrum is eliminated by using the (adjusted) radiation of a star of equal spectral type as a template in the spectral range of the studied HH line. This technique works especially well for forbidden lines; position-velocity diagrams are obtained for these lines of the stellar jet very close to the star. Radial velocities are given with respect to the photospheric velocity, the position is expressed in distances to the source star. From these diagrams we can sometimes obtain useful information about the outflow close to the star (up to a fraction of an arcsecond.) In figure 5 we show as an example the [S II]6731 position-velocity diagram covering the complex outflow environment of *T Tau* for the position angles 0 and 90 degrees. In the 90^o diagram we can clearly recognize a peak in intensity at ~ -130 km/sec which is extended in the negative direction (270^o) and increases in velocity up to -175 km/sec and is visible up to 3."5 from the star. The fact that the velocity dispersion for this component (B and B') is considerably smaller than the centroid radial velocity shows that this is a strongly collimated flow which is visible only 0."3 from *T Tau.* (Fig 5b.) This is the origin of the outflow which continues as HH 155 to at least 32" west of *T Tau* (Schwartz 1975, Bührke, Brugel & Mundt 1986, see also Reipurth 1994.) The position-velocity diagram for 0^o also shows a

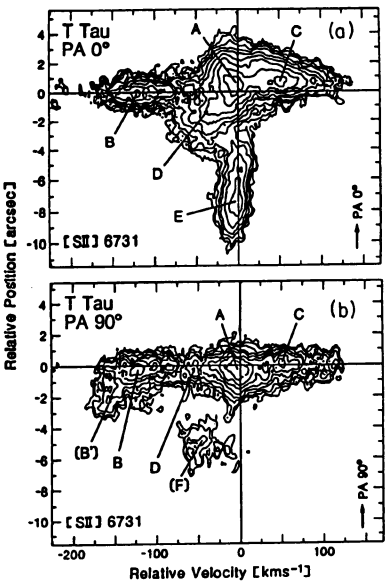

Figure 5. The position-velocity diagram for [S II]6731, indicating the kinematics of the different outflow systems in the immediate environment of T Tau using Solf's method. The upper diagram refers to a position angle 0°, The lower to a position angle of 90°. In the upper diagram we see the weakly collimated bipolar wind C, D. In the lower diagram we see the highly collimated jet (velocity dispersion $\ll$ centroid velocity) starting with v=−130 km/sec at 0."3 from the star and pointing in the direction 270° (B and B'). It is visible at large distance as HH155. The enigmatic main part (E) of Burnham's nebula has very low velocity and low velocity dispersion although it has a HEO shock wave spectrum. From Böhm and Solf's (1994) data.

(much less collimated) bipolar outflow in the directions 345°/165° (Böhm & Solf 1994.) The enigmatic properties of component E (the main part of Burnham's nebula – HH255) have been discussed by Böhm & Solf (1997).

6. Future Studies of HH Spectra

In the future it will be important to clarify the remaining general contradictions between spectrophotometric observations of certain lines in a large number of HH objects and the predictions of simple bow shock (or plane shock) models.

1) These include the unpredicted strength of the [S II] 6716,6731 lines for all high and intermediate excitation objects (as indicated by the [S II] 6716,6731/$H\alpha$ ratio.)

2) Another surprising feature is that the observed line ratios of high

https://doi.org/10.1017/S0074180900061532 Published online by Cambridge University Press

ionization lines, like [O III]5007/H_β and [NeIII]3869/H_β in all high excitation objects require a shock wave velocity not essentially larger than 120 km/sec which leads to the strange conclusion that there are many HH objects with shock velocities up to (say) 120 km/sec but that there are hardly any with shock velocities above this value. This effect is confirmed by line ratios observed in the UV.

It is obvious from 1) and 2) that there is a fundamental problem with the present bow shock model.

3) The unusually high flux in the C I 9850 line and the unexpected spatial distribution of this line in some low excitation objects should be studied and explained.

4) The apparently different pre-shock density for High Excitation Objects (mostly $N \sim 10^2/cm^3$) and Low Excitation Objects (mostly $N \sim 10^3/cm^3$) should be further studied. One should attempt to find HEO's with N comparable to those of LEO's.

5) It has been shown that the spectrophotometry and its interpretation in terms of abundances in HH objects can be carried out with considerable accuracy. The gas-phase metal abundance in HH shock waves should now be determined for fairly large numbers of HH objects to see whether there are objects with drastically reduced abundance due to grain formation.

6) With regard to the study of position-velocity diagrams we expect especially interesting results from a further application of Solf's method (1989) to the jet and shock wave structure in the immediate vicinity of the source star. While the obvious observations of this type have been made (see e.g. Hirth 1994), a more detailed interpretation may be extracted from these observations, such as establishing the correlation between kinematics and ionization, which has given useful insight in the case of *T Tau* (Böhm & Solf 1997; Hartigan, Edwards & Ghandour 1995.)

References

Bautista, M.A. & Pradhan, A.K.: 1995, ApJ 442, L65
Beck-Winchatz, B., Böhm, K.H. & Noriega-Crespo, A.: 1996, AJ 111,346
Biro, S. & Raga, A.C.: 1994, ApJ 434, 221
Blondin, J.M., Königl, A. & Fryxell, B.A.:1989, ApJ 337, L37
Böhm, K.H.: 1956, ApJ 123, 379
Böhm, K.H.: 1983, Rev Mex AA 7, 55
Böhm, K.H.: 1995 in Shocks in Astrophysics, ed. T. Millar & A. Raga (Dordrecht: Kluwer), p.11
Böhm, K.H., Böhm-Vitense, E. & Brugel, E.: 1981, ApJ 245, L113
Böhm, K.H., Brugel, E. & Mannery, E.: 1980, ApJ 235, L137
Böhm, K.H. & Solf, J.: 1990, ApJ 348, 297
Böhm, K.H. & Solf, J.: 1994, ApJ 430, 277
Böhm, K.H. & Solf, J.: 1997, A&A 318, 565
Bührke, T., Brugel, E.W. & Mundt, R.: 1986, A&A 164, 83

Cameron, M. & Liseau, R.: 1990, A&A 240, 409
Cantó, J. & Raga, A.C.: 1991, ApJ 372, 646
Davis, C.J., Eisloffel, J. & Ray, T.P.: 1994, ApJ 426, L93
Davis, C.J., Eisloffel, J. & Smith, M.D.: 1996, ApJ 463, 246
De Gouveia Dal Pino, E.M. & Benz, W.: 1993, ApJ 410, 686
Draine, B.: in Shocks in Astrophysics, ed. T. Millar & A. Raga (Dordrecht: Kluwer), p. 111
Dopita, M.: 1978, ApJS 37, 117
Dopita, M., Schwartz, R.D. & Evans, I.: ApJ 263, L73
Fernandes, A. Brand, P. & Burton, M.: 1995, in Shocks in Astrophysics, ed. T. Millar & A. Raga (Dordrecht: Kluwer) p. 45
Garstang, R.H., Robb, W.D. & Roundtree, S.P.: 1978, ApJ 222, 384
Hartigan, P., Raymond, J. & Hartmann, L.: 1987, ApJ 316, 323
Hartigan, P., Edwards, S. & Ghandour, L.: 1995, ApJ 452, 736
Hartmann, L. & Raymond, J.: 1984, ApJ 276, 560
Henney, W.J.: 1996, Rev Mex AA 32, 3
Henney, W.J., Raga, A.C. & Axon, D.J.: 1994, ApJ 427, 305
Herbig, G.H. 1951: ApJ 113, 697
Hirth, G.A. 1994: Ph.D. Thesis, University of Heidelberg
Hirth, G.A., Mundt, R. & Solf, J.: 1994, A&A 285, 233
Indebetouw, R. & Noriega-Crespo, A.: 1995, AJ 109, 752
Moro-Martin, A., Noriega-Crespo, A., Böhm, K.H. & Raga, A.C.: 1996, Rev Mex AA 32, 75
Noriega-Crespo, A., Calvet, N. & Böhm, K.H.: 1991, ApJ 379, 676
Noriega-Crespo, A., Garnavich, P.M., Raga, A.C., Cantó, J. & Böhm, K.H.: 1996, ApJ, 462, 804
Osterbrock, D.E.: 1958, PASP, 70, 399
Raga, A.C.: 1995, Rev Mex AASC 1, 103
Raga, A.C. & Böhm, K.H.: 1985, ApJS 58, 201
Raga, A.C. & Böhm, K.H.: 1986, ApJ 308, 829
Raga, A.C. & Böhm, K.H.: 1987, ApJ 323, 193
Raga, A.C., Böhm, K.H. & Cantó, J.: 1996, Rev Mex AA 32, 161
Raga, A.C., Mateo, M., Böhm, K.H. & Solf, J.: 1988, AJ 95, 1783
Raymond, J.: 1979, ApJS 39, 1
Raymond, J., Hartigan, P. & Hartmann, L.: 1988, ApJ 326, 323
Reipurth, B.: 1994, A general catalogue of Herbig-Haro objects, electronically published via ftp to hq.eso.org in directory /pub/catalogs/Herbig-Haro
Reipurth, B. & Cernicharo, J.: 1995, Rev Mex AASC 1, 43
Schwartz, R.D.: 1975, ApJ 195, 631
Schwartz, R.D.: 1983, ApJ 268, L87
Seab, C.G.: 1987, in Interstellar Processes, ed. D. Hollenbach & H. Thronson (Dordrecht: Reidel), p. 491
Solf, J.: 1989, in Low Mass Star Formation and Pre-Main Sequence Objects, ed. B. Reipurth (Garching: ESO Conf. Series 33), 399
Solf, J.: 1993, in Stellar and Circumstellar Astrophysics, ed. G. Wallerstein & A. Noriega-Crespo (San Francisco: ASP Conf. Series), p. 22
Solf, J. & Böhm, K.H. 1991: ApJ 375, 618
Solf, J. & Böhm, K.H. 1993: ApJ 410, L31
Solf, J., Böhm, K.H. & Raga, A.C.: 1986, ApJ 305, 795
Solf, J., Böhm, K.H. & Raga, A.C.: 1988, ApJ 334, 229
Solf, J., Raga, A.C., Böhm, K.H. & Noriega-Crespo, A.: 1991, AJ 102, 1147
Staude, H.J. & Elsasser, H.: 1993, A&AR 5, 165
Stone, J.M. & Norman, M.L.: 1993, ApJ 413, 198
Wolfire, M.G. & Königl, A.: 1991, ApJ 383, 205
Zhang, H.L. & Pradhan, A.K.: 1995, A&A 293, 95